Proceedings of the ASME 2010 Eighth International Fuel Cell Science, Engineering and Technology Conference
FuelCell2010
June 14-16, 2010, Brooklyn, New York, USA

FuelCell2010-33304

Transient Performance of Integrated SOFC System Including Spatial Temperature Control

Fabian Mueller†, Mahshid Fardadi, Brendan Shaffer, Jacob Brouwer, Faryar Jabbari
Mechanical and Aerospace Engineering Department
National Fuel Cell Research Center
University of California, Irvine
Irvine, CA 92697
† - corresponding author, tel: 949-824-6602, fax: 949-824-7423, email: fm@nfcrc.uci.edu

ABSTRACT

Spatial temperature feedback control has been developed for a simulated integrated non-pressurized simple cycle solid oxide fuel cell (SOFC) system. The fuel cell spatial temperature feedback controller is based on (1) feed-forward set-points that minimize temperature variation in the fuel cell electrode- electrolyte solid temperature profile for the system operating power range, and (2) decentralized proportional-integral based feedback to maintain the fuel cell spatial temperature profile during transients and disturbances. Simulation results indicate the fuel cell spatial temperature variation can be maintained within 15 degrees of nominal to significant load perturbations.

Temperature gradients through the fuel cell are needed to remove the heat generated within the cell and cannot be avoided. The goal of the developed spatial temperature control is to minimize temperature variations from a nominal temperature profile in time. Minimal temperature variations in the SOFC electrode-electrolyte solid assembly will result in decreased thermal stresses and thereby decreased degradation and probability-of-failure. Simulation results demonstrating the ability to maintain the SOFC spatial temperature during large load perturbations indicates SOFC could be designed and controlled for rapid load following capability. Such performance can greatly improve SOFC system operating flexibility and thereby open new markets for SOFC systems including load following or spinning reserve services for the utility grid.

KEY WORDS: SOFC, integrated system, dynamic simulation, transient performance, fuel cell system control, dynamic response

INTRODUCTION AND BACKGROUND

Solid oxide fuel cells have rapid load following capability, on the time-scale of electrochemical kinetics. The challenge is that all of the system balance-of-plant components must be operated in unison to support operation of the rather delicate fuel cell stack while maximizing efficiency and minimizing degradation and probability of failure.

Due to these challenges, the transient operation of SOFC has not yet been successfully demonstrated in the field. However, dynamic models of integrated SOFC system models have been developed to evaluate the transient performance of various system configurations and system controls [1-7]. Developed models have been verified to limited available integrated SOFC operation data [4, 8-10]. Prior, simulation efforts have indicated that with proper system design and system control, the operating conditions of the SOFC systems can be maintained during transient operation [3, 4, 6, 7]. Key issues that must be addressed to enable SOFC load following include:

Steam to carbon ratio: Most practical solid oxide fuel cell systems will typically operate on natural gas or biogas. To avoid carbon coking of the fuel cell and reformer, sufficient steam must be mixed with the carbon based fuels. In the past, steam to carbon ratios; have been maintained either by recirculating depleted fuel, which contain steam, or by injecting steam with the fuel. In either case, sufficient inlet steam must be ensured to avoid carbon coking of the fuel cell and reformer.

Reformer flow delay: Fuel flow delays in the reformer, can cause the fuel to be depleted in the fuel cell following a load transient. Flow delays in the reformer should be minimized, and a governor should be placed on the fuel cell current to ensure the fuel in the fuel cell does not deplete (for a good discussion see Gaynor et. al [5]).

High reformer temperature: If the system contains an external fuel reformer, the temperature of the reformer should be maintained for all operating conditions. Since, steam reformation is endothermic; the reformer heat source must be maintained for sustained chemical conversion. In most systems

this can be achieved by heating the reformer with sufficiently hot depleted fuel combustor exhaust.

High cathode inlet air temperature: The fuel cell cathode inlet temperature must be maintained. A challenge is that for increased efficiency as much of the exhaust heat from the system must be recuperated, but only limited high temperature heat is available to achieve both high anode and cathode inlet flows. SOFC system configurations vary greatly in approaches to achieve both high anode and cathode inlet temperatures, with the challenge being primarily on the cathode side, since cathode air flow is much greater than the anode fuel flow. Thermal integration techniques include, recirculating air via either an ejector or blower, heat exchanger networks, and innovative combustor designs.

Cathode air flow manipulation: The amount of heat generated in the fuel cell will vary with the fuel cell operating power, and operating condition. To thermally control the fuel cell, the amount of air flow through the fuel cell must be manipulated. This can be achieved, by varying blower or compressor air flow, by bypassing air around the fuel cell, or by varying the amount of air recirculation.

Cathode inlet temperature manipulation: To manage the fuel cell temperature profile it is advantageous to have independent control of air flow rate as well as the cathode inlet temperature. Two actuators are required for independent control of the air flow and inlet temperature. One approach as is explored herein is variable speed blower to vary the air flow, and a variable air bypass around the air recuperator.

Combustor temperature control: While the fuel cell is the most delicate component of a SOFC system, the fuel cell air flow, fuel flow, and fuel cell electrochemistry all will impact the combustor that oxidizes the fuel cell depleted fuel. Without special consideration, significant combustor temperature dynamics will be observed in the combustor following load or disturbance perturbations. The combustor temperature can be controlled by varying the fuel cell fuel and/or air utilization.

Due to the considerations as explained above, an integrated system control strategy is required to control the fuel cell system following load perturbations. Various response time scales impact the fuel cell. Thermal response are on the order of seconds to hours, while species concentration of reacting flows are on the order of seconds, and chemical and electrochemical kinetics are on the order of milliseconds. Variations in the time scale allow control loops to be considered independently for synthesis even though the control loops can be coupled. Typically at least three control loops are required with respect to the three primary manipulated variables.

1. Fuel cell current - system power control loop
2. Fuel flow – fuel cell utilization – combustor temperature control loop
3. Air flow – fuel cell thermal management control loop

Transient operation, and spatial temperature control is developed herein based on an integrated SOFC dynamic model previously developed for controls evaluation [3, 4, 11]. Previous control efforts have demonstrated that with novel controls, the fuel cell anode fuel concentration, average temperature, and combustor temperature could all be maintained during load transients. The main limitation however, of the previously presented work is that a bulk SOFC model was used. To minimize fuel cell thermal fatigue and probability of failure as is explored by Nakajo [12, 13], it is desired to minimize temperature variations in the fuel cell solid in time.

INTEGRATED SYSTEM

The system configuration evaluated in this study is that same as explored in [3, 4, 11] (as represented in Figure 1). The system is designed to operate in a power operating range between 3 to 5.5 kW. The fuel cell operates at ambient pressure from externally steam reformed natural gas. A variable speed blower is used, such that the air flow can be manipulated for fuel cell thermal management. The air is preheated using the combustor exhaust. Two air-exhaust heat exchangers are utilized; a high temperature (ceramic) heat exchanger and a stainless steel heat exchanger. The reformer is integrated between the two air heat exchangers, to ensure sufficient high temperature for the reformer. To control the cathode inlet temperature, air can bypass the heat exchangers. Water required for fuel reformation is supplied to the system from an external source. A steam preparation boiler is used to vaporize liquid water to steam using low temperature exhaust. To minimize thermal gradients in the fuel cell and risk of carbon coking in the fuel cell, the natural gas-steam stream is externally reformed to the fuel cell. In the presented configuration the reformer temperature is sufficient to ensure more than 90% methane conversion to hydrogen and carbon monoxide in the reformer. Details regarding the system balance of plant can be found in [3, 4, 11].

Using the same dynamic modeling methodology a spatial dynamic model of the fuel cell was added to the system as described in the next section. Further, a first order, 0.1 second delay was added to the bypass valve. The simulated system is among the simplest system that can be developed for robust yet flexible operation.

SOFC MODEL

The SOFC model is in the co-flow configuration and includes internal reformation. Each channel of the fuel cell is assumed to be the same, and only one channel of the fuel cell is modeled to give a quasi-two dimensional model. Finite volumes discretize the SOFC along the flow direction as well as in the vertical direction such that there are 24 nodes each containing four control volumes: PEN, interconnect, anode and cathode gases. This discretization reduces the partial differential equations to ordinary differential equations in time that can be solved using Matlab Simulink's ode15s solver. The finite control volume approach approximates the physical processes occuring in the fuel cell better than other methods

(Ferguson, 1996) [14]. Mass and energy are the conserved quantities; momentum is assumed constant. This assumption has been shown to affect the modeling results only slightly (Iora, 2005) [15]. The model makes other assumptions including:

1. The fuel cell is well insulated such that heat loss from the cell is negligible.
2. The flow in the fuel cell is laminar.
3. Pressure drops are negligible.
4. The gases are ideal and incompressible.
5. Radiation heat transfer is negligible. (Daun, 2006; Tanaka, 2007) [16, 17]
6. Conduction along the PEN is negligible since conduction through the interconnect dominates.
7. Coking is negligible due to high steam to carbon ratio. (Sangtongkitcharoen, 2005; Laosiripojana, 2007) [18, 19]
8. The water gas shift reaction is assumed to be in equilibrium.
9. Both electrodes exhibit high enough conductivity that it is assumed that both are an equi-potential surface.
10. Only hydrogen participates in the electrochemical reaction at the anode.
11. The electrochemistry is rapid such that the rate of reaction is proportional to the current.

Similar assumptions have been made by Mueller (2006) and Shaffer (2009) [20, 21]. Key SOFC model parameters can be found in Table 1.

ELECTROCHEMICAL MODEL

The electrochemical model relies on the equipotential assumption wherein the cell voltage is specified and the current of each node is adjusted such that the specified voltage is met.

$$V = E_{OCV} - \eta_{act} - \eta_{ohm} - \eta_{conc}$$

In the equation above, the open circuit voltage is calculated using the Nernst equation.

$$E_{Nernst} = E_0 - \frac{R_u T_{PEN}}{nF} \ln\left(\frac{P_{H2O}}{P_{H2} P_{O2}^{1/2}}\right)$$

The reversible potential E_o is defined as:

$$E_0 = -\frac{\Delta G}{nF}$$

Where the change in Gibb's Free Energy is calculated based on temperature from JANNAF thermo chemical tables.

The remaining terms in the equation for working voltage are the polarizations: activation, ohmic, and concentration.

The activation polarization (η_{act}) equation is shown below and has been derived from the Butler-Volmer model with the assumption of a transfer coefficient of 0.5.

$$\eta_{act,i} = \frac{2R_u T_{PEN}}{nF} \sinh^{-1}\left(\frac{I}{2 j_{0,i} A}\right)$$

The exchange current densities (j_o) for the anodic and cathodic reactions are calculated using the expressions developed by Ni et. al (2009) [22].

$$j_{o,an} = k_{an} \frac{1-\varepsilon}{r_p} exp\left(\frac{E_{act,an}}{RT}\right)$$

$$j_{o,c} = k_c \frac{1-\varepsilon}{r_p} exp\left(\frac{E_{act,c}}{RT}\right)$$

In the above equations, rp is pore size; ε is porosity; Eact,i is the activation energy; and ki is the pre-exponential constant that was chosen to fit experimental data.

The ohmic polarization model was developed from experimental data acquired by Kim et. al (1999) [23].

$$\eta_{ohm} = iR_{PEN}(T_{PEN})$$

$$R_{PEN} = T_{PEN} \cdot e^{C1/T_{PEN} + C0}$$

The constants C1 and C0 in the above equation were adjusted to fit the experimental data collected by Kim et. al (1999) [23].

The concentration polarization model is shown below and has been used by previously within the literature [2, 4, 20, 21, 24-26].

$$\eta_{conc} = -\frac{R_u T_{PEN}}{nF} \ln\left(1 - \frac{I}{j_L A}\right)$$

REFORMATION REACTIONS

The internal reformation is described by the reactions shown below and the chemical kinetics developed by Achenbach (1994) [27].

$$CH_4 + H_2O \rightarrow CO + 3H_2$$

$$CO + H_2O \rightarrow CO_2 + H_2$$

The reaction rate expression for the steam methane reformation reaction developed by Achenbach (1995) is below.

$$R = \pm \nu k_0 P_{CH4} A \left(1 - \frac{Q}{K_{eq}}\right) e^{-E_a / R_u T}$$

The coefficient ν is the stoichiometric coefficient of the particular species; the pre-exponential factor k_0 is 4.274 kmol/(m^2-s-bar); the partial pressure of methane is P_{CH4} in bars; A is the surface area of the node; Q is the reaction quotient; K_{eq} is the equilibrium constant; the activation energy E_a is 82,000 kJ/kmol; the universal gas constant R_u is 8.314 kJ/(kmol-K); and T is the temperature of the node.

The water gas shift reaction is assumed to be at equilibrium as mentioned previously. Ahmed (2000) [28] examined this assumption experimentally in their publication and found it to be true for typical SOFC conditions and at high levels of fuel utilization. For low levels of fuel utilization it was found that the WGS reaction did not approach equilibrium. The rate of reaction for the WGS reaction is shown below

$$R = \pm \nu k_0 P_{CO} A \left(1 - \frac{Q}{K_{eq}}\right)$$

and was adapted from Aguiar (2004) [29] where the pre-exponential constant, k_0, is a number large enough such that the rate of reaction equation is representative of equilibrium.

For the equations of conservation of energy and mass, see [2, 4, 20, 21, 24-26].

SYSTEM CONTROLLER

The goal is to develop a controller that (1) minimizes system power tracking error, (2) maintains the system operating conditions, and (3) minimize probability of failure and system degradation. The fuel cell control system is comprised of three primary integrated control loops, power, combustor temperature, and thermal management control loops as described in the introduction. The system power is controlled by manipulating the current, the combustor temperature is controlled at 1250 K for the whole range of operating power by manipulating the system fuel flow, and the blower speed, and heat exchanger bypass is manipulated to control the fuel cell spatial temperature distribution. Note by maintaining the combustor temperature it has been shown in [3, 4] that the fuel cell utilization can be maintained. Both the combustor and system power control loops are based on standard feed-forward (e.g., power demand based look up tables), and proportional – integral feedback as shown in Figure 2. More details and discussion regarding the fuel and system power control loops can be found in [3, 4].

The complete integrated system controller is represented in Figure 3. Not that the external input is the set-point system power between 3 to 5.5 kilowatts. The control system uses feed-forward look up tables and feedback to manipulate the fuel flow, fuel cell current, blower power, and heat exchanger bypass to match the system power set-point, and control the system to minimize degradation. The actuator value will change substantially with power demand. The look-up tables manipulate the actuators before the system physically responds. For example, following a load increase it can take a few seconds for the fuel within the fuel cell to deplete and the combustor temperature to vary. Hence, feed-forward actuation will increase the fuel cell fuel flow following a load demand increase before the fuel cell fuel content reduces thereby reducing the system transient variation following load perturbation. Because, other disturbances, system transient, and system degradation can also affect the system, it is beneficial to supplement feed-forward with feedback.

Similar integrated system controllers have been explored in [3, 4]. Here, we focus on the development of the fuel cell spatial temperature controller, to minimize fuel cell thermal fatigue.

With independent control of the air flow rate, and air inlet temperature, it is possible to obtain various fuel cell PEN operating temperatures and profiles within the system power range, operational reformer temperature, and controlled combustor temperature. To minimize thermal fatigue and probability of failure in the fuel cell, the goal is to minimize PEN temperature variations from nominal power temperature profile. In other words, to minimize thermal fatigue it is ideal to maintain the same solid PEN temperature profile over time for all operating power.

In the presented research 5 kilowatts was determined as the nominal operating point with a 1050 K to 1150 K inlet to outlet PEN temperature profile (in the fuel and air co-flow direction). The air flow and inlet air temperature at 3, 4 and 5.5 kilowatts were determined to minimize the temperature deviation from the nominal 5 kW temperature profile. The steady state PEN temperature profile at the 5 kW nominal operating condition, as well as 3, 4, and 5.5 kW system power set-point is shown in Figure 4.

It can be observed that the temperature profile cannot be maintained exactly. This result is expected since the amount of heat that must be removed from the fuel cell changes with power and many factors including the electrochemical reaction distribution (current), chemical reaction (steam reformation), and convective heat transfer between the PEN and air flow change non-linearly with power. However, the peak steady-state temperature deviation for the whole operating range to the nominal temperature profile is 11 degrees at 3 kW. By manipulating both the air flow, and air inlet temperature the fuel cell spatial temperature can well be maintained for a wide range of operating powers. Similar results have been developed previously for a single fuel cell by Fardadi et al., 2010 [30] but never before for an integrated system. While the steady-state performance of a single cell was expected to be reproducible for a system, the integrated system accounts for variation in the fuel flow utilization (to maintain constant combustor temperature) as well as anode inlet temperature variation.

As can be observed from a single cell optimization, it is important to note that the cathode inlet temperature increases with increasing power to maintain the same temperature profile (as was also observed in Fardadi et al. -2010 [30]). On an energy balance point of view, this is counterintuitive, since lower air inlet temperatures would result in heat removal from the fuel cell. However, to maintain the spatial temperature profile, the air inlet temperature should be increased with increasing power.

The key system operating parameters for the spatial temperature optimized case are shown in Figure 5. It can be seen that the air flow and blower power does not increase linearly with system power. Nonetheless high system efficiencies (increasing at part load condition) can be achieved for the whole system operating range.

The steady-state optimization is used to determine the operating conditions that minimize PEN spatial temperature deviation from the nominal operating condition. The feed-forward look-up tables and temperature set-points are determined from the steady state optimization. Feedback loops are needed to maintain the system during transients, and to disturbances. Prior, work by Fardadi et al. 2010 [30] has used H-infinite feedback synthesis to develop a feedback controller, which actually did not use any feed-forward. Here we develop a simplified SISO based feedback controller. Fuel cell companies may not have (1) an accurate numerical model of the system, and (2) the in-house control expertise to synthesize such a control system. Using a simplified feedback control system control approach the control system can potentially be tuned from field testing of SOFC systems, even though a dynamic model can provide substantial insight.

OPEN LOOP RESPONSE

It is critical to understand that a feedback loop is required to supplement feed-forward due to system transients and

disturbances. Figure 6, shows the fuel cell spatial temperature response to a 3 to 5.5 kW load increase with only feed-forward actuation. The PEN temperatures at the air inlet overshoot nearly 50 degrees following the perturbation. At lower power, the air recuperator and fuel reformer operate at a higher temperature. Following a load perturbation, with only feed-forward actuation, the fuel cell anode and cathode flow is temporarily hotter as the balance-of-plant cools. The hotter than steady-state inlet anode and cathode flow temperatures; result in the observed PEN temperature transient. The balance-of-plant thermal capacitance induced substantial PEN temperature variations may not be acceptable. The good news is feedback control can help reduce the temperature transient.

With multi input multi output control case, the whole temperature profile can be controlled. However, in the SISO case, the number of control parameter is limited by the number of actuators. In the current system configuration only two PEN temperature parameters can be controlled, in coupled but separate control loops since two actuators are available: the variable speed blower and heat exchanger bypass.

HEAT EXCHANGER CASCADE CONTROLLER

By manipulating the heat exchanger bypass it is possible to control the cathode inlet air temperature. It is important to remember that the bypass valve can be used to decrease the inlet temperature, but that the inlet temperature is limited by the exhaust gas temperature and effectiveness of the heat exchanger (i.e., with the bypass valve fully closed). The heat exchangers must be sufficiently sized, to achieve the required cathode inlet temperature.

In the presented research, the bypass is used to control the PEN inlet temperature. This is because the cathode inlet temperature will most directly affect the PEN inlet temperature, and peak temperature disturbances tend to happen at the air inlet and outlet of the fuel cell (even though peak temperature deviation can also take place at the middle of the cell). To control the PEN inlet temperature, a cascade controller is used as shown in Figure 7 where the bypass valve is manipulated to control a cathode inlet temperature, which is manipulated to control the PEN inlet temperature. By using this cascade structure, the bypass can mitigate inlet air temperature transients from the balance of plant thermal capacitance.

From simulation trial and error it was found that delaying the feed-forward with a first order 40 second delay greatly minimized PEN spatial temperature deviation from the nominal temperature profile. Rapid feed-forward bypass manipulations were found to interact with the blower cascade controller and cause oscillations. Further, the natural response of the PEN temperature is not instantaneous. Hence, trying to rapidly control the PEN temperature to steady-state value resulted in increased temperature variations.

BLOWER CASCADE CONTROLLER

Prior work [3, 4] has shown that a cascade blower power, blower RPM, PEN temperature cascade controller as shown in Figure 8 is beneficial. In such a controller the blower power is manipulated to maintain a blower RPM set-point, which is manipulated to thermally manage the PEN. The cascade controller that directly controls the blower speed serves to compensate for the blower inertia by manipulating the blower power, improving control over the fuel cell air flow.

With only two actuators (i.e., blower and heat exchanger bypass), only two PEN temperature parameters can be controlled with single-input-single-output control. Further, the heat exchanger bypass and blower flow rate control loops will interact. Using the developed dynamic model different input output pairing was evaluated. For example, the heat exchanger bypass was used to control the PEN air inlet temperature, and the blower to control the PEN air exit temperature. The system response to a 5.5 kW to 3 kW load decrease is shown in Figure 9. Note that a feed-forward and feedback controller is used. The system response oscillated, due to control loop interactions between the heat exchanger bypass and blower speed control loops. With this pairing, the only way the oscillations could be removed was to increase the feedback gain of one loop and decreasing the gain of the other. In other word one of the two feedback loops had to be removed, or substantially minimized.

Understanding this interaction in more detail is subject to further research, but it is clear that the two control loops are interacting, which makes sense from a system physical understanding. Both actuators impact both the PEN inlet and outlet temperatures, and the actuator response to temperature variations depend on the operation of the other actuators. Further, both actuators respond at slightly different time scales and are both prone to saturate making for a difficult control problem. Some level of information between each control loop must be shared to achieve a stable multi-loop controller.

A centralized H-infinite or LQR controller can be developed as in Fardadi et al. 2010 . However, through some trial and error of input-output pairing in the dynamic model, it was found that decent temperature controller could be achieved by paring the heat exchanger bypass to the PEN air inlet temperature, and the blower to the average of the PEN inlet and outlet temperature (Ti+Tf)/2. The system performance to a 5.5 kW to 3 kW load decrease is shown in Figure 10. With the new input output pairing the control interactions and oscillations are substantially decreased (with the same feedback gains), even though the interactions still exist.

SIMULATION RESULTS

Pairing the heat exchanger bypass to the PEN inlet temperature and blower to the average PEN inlet and outlet temperature was the best control pairing that was found. The system performance is evaluated with this control pairing in the rest of the paper; however future work is required to evaluate other pairing, shared information between control loops, controller loop shaping and anti-windup controllers during saturation, all which can result in increased system performance.

LOAD DECREASE

The goal of the temperature control loops is to minimize PEN temperature variations from the nominal 5 kW PEN temperature profile. It was found from open loop analysis that feedback control is beneficial to minimize the impact of the balance of plant thermal inertia on the PEN temperature response. Two actuators are available to control the PEN

temperature profile, the heat exchanger bypass and variable speed blower. It was found that the two actuators are inter-coupled and individual feedback loops will interact. This leads to an interesting control tradeoff where a larger feedback gain is desired to reject system transient disturbances on the system following a load decrease but smaller feedback gains to minimize control interactions between the two control loops.

A sensitivity analysis was conducted on the feedback gain magnitude to minimize the PEN spatial temperature deviation in time following a system load decrease from 5.5 to 3 kW. Temperature control error of the PEN inlet, PEN outlet, and combustor temperature are shown on a semi log scale in Figure 11 for two control gains. Before the specific sensitivity of the feedback gain is discussed different system time scales are explained. The system temperature response is impacted by a large range of time scales, control design features and system physical response as indicated in the figure. Initially the combustor temperature increases as electrochemical reaction decreases before the fuel flow. Consequently the air flow and temperature impact the combustor temperature (see [3, 4] for more discussion).

On the other hand, the PEN temperature does not respond on the sub second time scale, but gets impacted by the temperature controller set-point, the balance of plant thermal inertia (e.g., recuperator) increasing the inlet air temperature, as well as controller interactions, and controller integrator driving the temperature error to zero.

With smaller feedback gain, the balance of plant inertia results in an increased temperature controller error at the PEN inlet. Some controller interactions take place after the initial temperature deviation, but the temperature stabilizes. With larger feedback gains, the initial temperature variation at the PEN inlet can be decreased, however, subsequent controller interactions can result in larger temperature deviations, and increased temperature oscillations. Hence, it is suggested to tune the feedback gain to minimize the peak PEN controller error but avoid oscillations at all cost.

The nodal PEN temperature response to the 3 to 5.5 kW load decrease is shown in Figure 12Figure 12 for the smaller feedback gains. Some temperature overshoot due to the system set point temperature changing and the system inertia is present, but overall the temperature response monotonically. The peak temperature deviation is maintained within 15 degrees from nominal for the entire thermal response to the load decrease.

LOAD DECREASE

To further demonstrate the performance of the controller, the system performance and temperature response to a 3 to 5 kilowatts load increase is presented in Figure 14 and Figure 13 respectively. The rapid system power demand increase is tracked almost exactly, with maintained fuel cell voltage and currents. The blower speed and power responds to PEN temperature deviation but overall is well maintained. The PEN inlet temperature overshoot slightly but good overall temperature control was established.

DISCUSSION AND CONCLUSION

The dynamic modeling simulations indicate that SOFC can potentially load follow with limited temperature variations. Decreasing temperature deviations can substantially reduce probability of cell failures and reduce thermal fatigue within the fuel cell.

To minimize temperature deviation from the nominal temperature profile, both the air inlet temperature and the air flow through the fuel cell must be manipulated. With feedback on both actuators, some level of actuator interactions will take place. Good system transient performance was demonstrated to both load increase and decrease perturbations, but potential for further improvement is apparent by use of centralized control, loop shaping and saturation anti wind up.

The authors believe the simulated transient performance can be demonstrated in a commercial system, but such will require developing a dynamic model and specific control system for the unit. For economic viability, high temperature fuel cells should be normally operated at full power. However, during contingency conditions it may be possible to inland buildings or micro-grids served by high temperature fuel cells with transient capability as demonstrated here. Also, decreased load demands and low night time electric rates may make drive for economical part-load nigh time operation. While significant control development is needed, only limited hardware modification is required to enable load following. Further, controls can decrease fuel cell thermal degradation and probability of failure.

Acknowledgement

The authors graciously acknowledge the partial financial support for this work that was provided by the California Energy Commission under the Energy Innovations Small Grant number 56017A/08-09.

REFERENCES

1. Mueller, F., et al. *Dynamic Simulation of an Integrated Solid Oxide Fuel Cell System Including Current-Based-Fuel Control*. in *International Conference on Fuel Cell Science, Engineering and Technology*. 2005. Ypsilanti, MI: ASME.
2. Mueller, F., et al. *Control Design for A Bottoming Solid Oxide Fuel Cell Gas Turbine Hybrid System*. in *Fuel Cell Science, Engineering and Technology*. 2006. Irvine, CA: ASME.
3. Mueller, F., et al., *Novel solid oxide fuel cell system controller for rapid load following.* Journal of Power Sources, 2007. **172**(1): p. 308-323.
4. Mueller, F., *The Dynamics and Control of Integrated Solid Oxide Fuel Cell Systems: Transient Load-Following and Fuel Disturbance Rejection*, in *Mechanical and Aerospace Engineering*. 2008, University of California, Irvine: Irvine.
5. Gaynor, R., et al., *On Control Concepts to Prevent Hydrogen Starvation in Solid Oxide Fuel Cells.* Journal of Power Sources, 2008. **180**(1): p. 330-342.
6. Mueller, F., et al. *Design, Simulation and Control of a 100 Megawatt Class Solid Oxide Fuel Cell Gas Turbine Hybrid System*. in *6th International Fuel Cell Science, Engineering and Technology Conference*. 2008. Denver, Colorado: ASME.
7. Mueller, F., et al., *Synergistic integration of a gas turbine and solid oxide fuel cell for improved transient capability.* Journal of Power Sources, 2008. **176**(1): p. 229-239.
8. Brouwer, J., et al., *Analysis of a molten carbonate fuel cell: Numerical modeling and experimental validation.* Journal of Power Sources, 2006. **158**(1): p. 213-224.
9. Roberts, R. and J. Brouwer, *Dynamic Simulation of a Pressurized 220 kW Solid Oxide Fuel-Cell-Gas-Turbine Hybrid System: Modeled Performance Compared to Measured Results.* Journal of Fuel Cell Science and Technology, 2006. **3**(18): p. 18-25.
10. Mueller, F., et al., *Dynamic Simulation of an Integrated Solid Oxide Fuel Cell System Including Current-Based Fuel Flow Control.* Journal of Fuel Cell Science and Technology, 2006. **3**(2): p. 144-155.
11. Mueller, F., *On the Intrinsic Transient Capability and Limitations of Solid Oxide Fuel Cell Systems.* Journal of Power Sources, 2009. **187**(2): p. 452-460.
12. Nakajo, A., et al., *Simulation of thermal stresses in anode-supported solid oxide fuel cell stacks. Part I: Probability of failure of the cells.* Journal of Power Sources, 2009. **193**(1): p. 203-215.
13. Nakajo, A., et al., *Simulation of thermal stresses in anode-supported solid oxide fuel cell stacks. Part II: Loss of gas-tightness, electrical contact and thermal buckling.* Journal of Power Sources, 2009. **193**(1): p. 216-226.
14. Ferguson, J.R., J.M. Fiard, and R. Herbin, *Three-dimensional numerical simulation for various geometries of solid oxide fuel cells.* Journal of Power Sources, 1996. **58**(2): p. 109-122.
15. Iora, P., et al., *Comparison of two IT DIR-SOFC models: Impact of variable thermodynamic, physical, and flow properties. Steady-state and dynamic analysis.* Chemical Engineering Science, 2005. **60**(11): p. 2963-2975.
16. Daun, K.J., et al., *Radiation heat transfer in planar SOFC electrolytes.* Journal of Power Sources, 2006. **157**(1): p. 302-310.
17. Iwahara, H., et al., *Prospect of hydrogen technology using proton-conducting ceramics.* Solid State Ionics, 2004. **168**(3-4): p. 299-310.
18. Sangtongkitcharoen, W., et al., *Comparison of carbon formation boundary in different modes of solid oxide fuel cells fueled by methane.* Journal of Power Sources, 2005. **142**(1-2): p. 75-80.
19. Laosiripojana, N., S. Assabumrungrat, and S. Charojrochkul, *Steam reforming of ethanol with co-fed oxygen and hydrogen over Ni on high surface area ceria support.* Applied Catalysis A: General, 2007. **327**(2): p. 180-188.
20. Mueller, F., *Design and Simulation of a Tubular Solid Oxide Fuel Cell System Control Strategy*, in *Mechanical and Aerospace Engineering*. 2006, University of Californina, Irvine: Irvine.
21. Shaffer, B., Hunsuck, M., Brouwer, J., *Quasi-3-D Dynamic Model of an Internally Reforming Planar Solid Oxide Fuel Cell for Hydrogen Co-Production*, in *ASME Fuel Cell Science, Engineering, and Technology*. 2008, ASME: Denver, CO.
22. Ni, M., D.Y.C. Leung, and M.K.H. Leung, *Electrochemical modeling and parametric study of methane fed solid oxide fuel cells.* Energy Conversion and Management, 2009. **50**(2): p. 268-278.
23. Kim, J.-W., et al., *Polarization Effects in Intermediate Temperature, Anode-Supported Solid Oxide Fuel Cells.* Journal of The Electrochemistry Society, 1999. **146**(1): p. 69-78.
24. Auld, A.E., et al., *Applications of one-cycle control to improve the interconnection of a solid oxide fuel cell and electric power system with a dynamic load.* Journal of Power Sources, 2008. **179**(1): p. 155-163.
25. Gaynor, R., et al., *On control concepts to prevent fuel starvation in solid oxide fuel cells.* Journal of Power Sources, 2008. **180**(1): p. 330-342.
26. Roberts, R., et al., *Control design of an atmospheric solid oxide fuel cell/gas turbine hybrid system: Variable versus fixed speed gas turbine operation.* Journal of Power Sources, 2006. **161**(1): p. 484-491.
27. Achenbach, E., *Three-dimensional and time-dependent simulation of a planar solid oxide fuel cell stack.* Journal of Power Sources, 1994. **49**(1-3): p. 333-348.
28. Ahmed, K. and K. Foger, *Kinetics of internal steam reforming of methane on Ni/YSZ-based anodes for solid oxide fuel cells.* Catalysis Today, 2000. **63**(2-4): p. 479-487.
29. Aguiar, P., C.S. Adjiman, and N.P. Brandon, *Anode-supported intermediate-temperature direct internal reforming solid oxide fuel cell: II. Model-based*

dynamic performance and control. Journal of Power Sources, 2005. **147**(1-2): p. 136-147.

30. Fardadi, M., F. Mueller, and F. Jabbari, *Feedback control of solid oxide fuel cell spatial temperature variation.* Journal of Power Sources. **In Press, Corrected Proof**.

TABLES

Table 1 SOFC model parameters

Parameter	Value	Units
PEN thickness	1.06	mm
PEN Density	5900	kg/m^3
PEN Specific Heat	0.5	kJ/kg-K
PEN Thermal Conductivity	2	W/m-K
IC thickness	4	mm
IC Density	9000	kg/m^3
IC Specific Heat	0.62	kJ/kg-K
IC Thermal Conductivity	25	W/m-K
C1	7509.6	
C0	-25.855	
k_{an}	325	
k_c	1157	cm^2
j_L	10000	A/m^2
$E_{act,an}$	1.00E+05	kJ/kmol
$E_{act,c}$	1.20E+05	kJ/kmol
j_L	9000	A/m^2
Cathode Channel Ht.	2	mm
Anode Channel Ht.	1	mm
Cell Width	10	cm
Cell Length	10	cm
Channel Width	2.5	cm
Rib Width	0.5	mm
Cell Length	10	cm

FIGURES

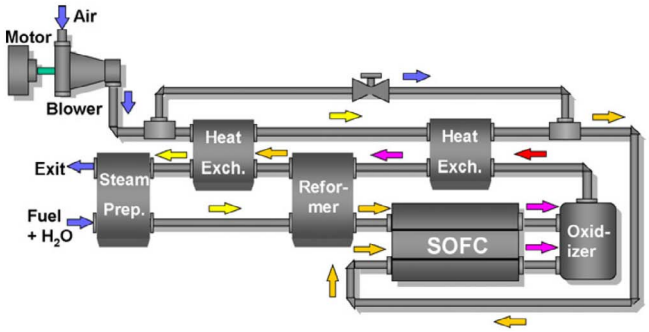

Figure 1 Schematic of the nominal 5 kW integrated SOFC system

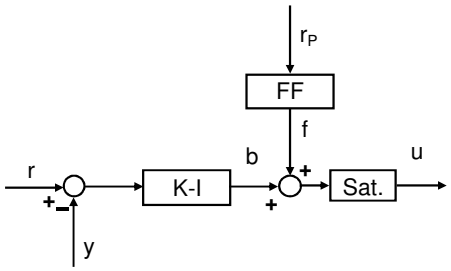

Figure 2 Standard feed-forward feedback control loop

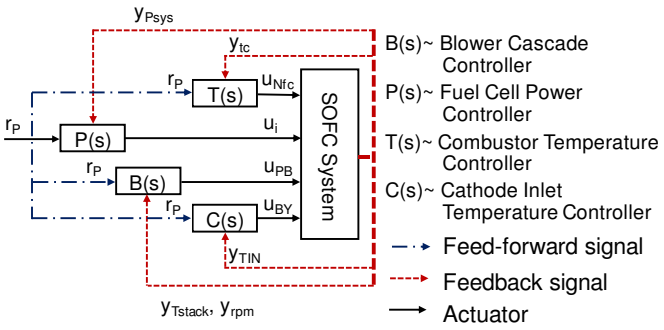

Figure 3 Integrated system controller.

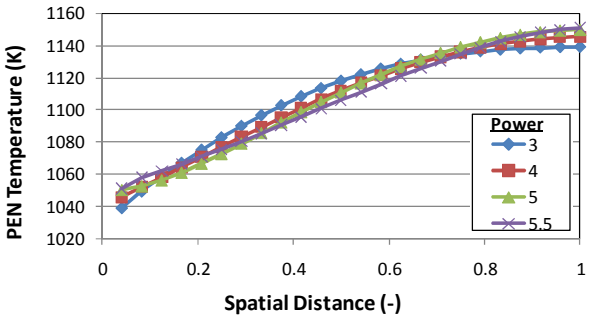

Figure 4 Steady-state PEN part load spatial temperature profiles

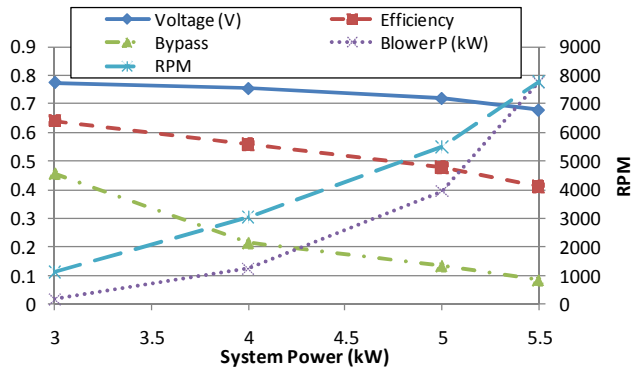

Figure 5 System part load operating performance.

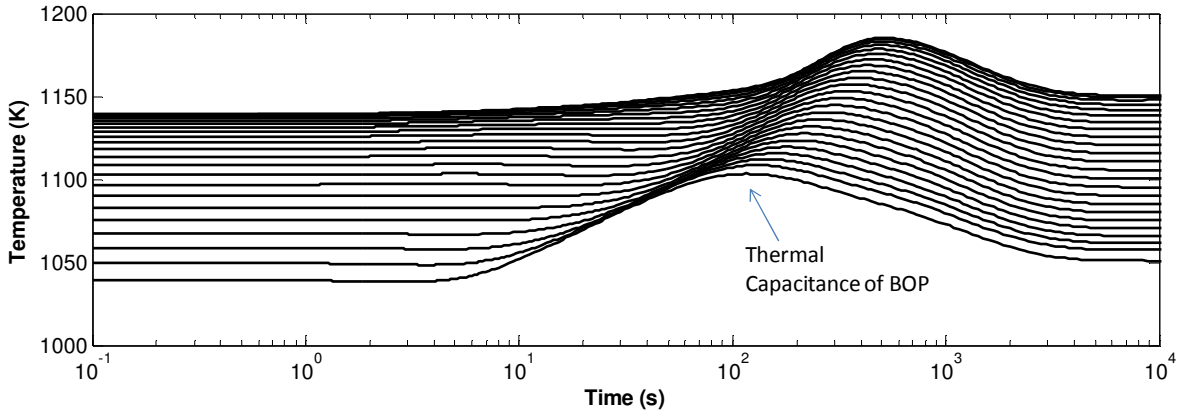

Figure 6 Open loop response to a 3 to 5.5 kW load increase.

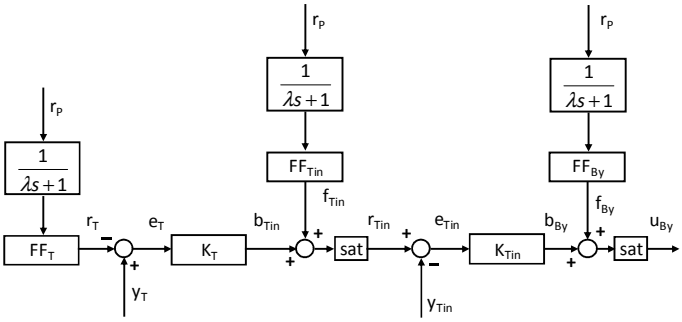

Figure 7 Heat exchanger bypass cascade controller

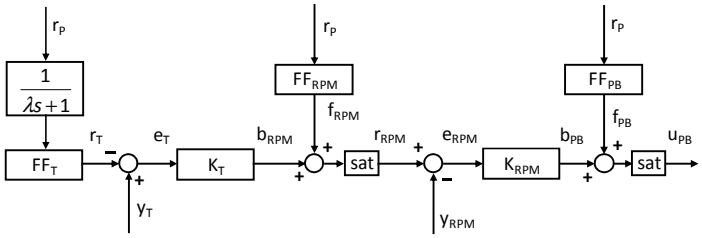

Figure 8 Blower cascade controller.

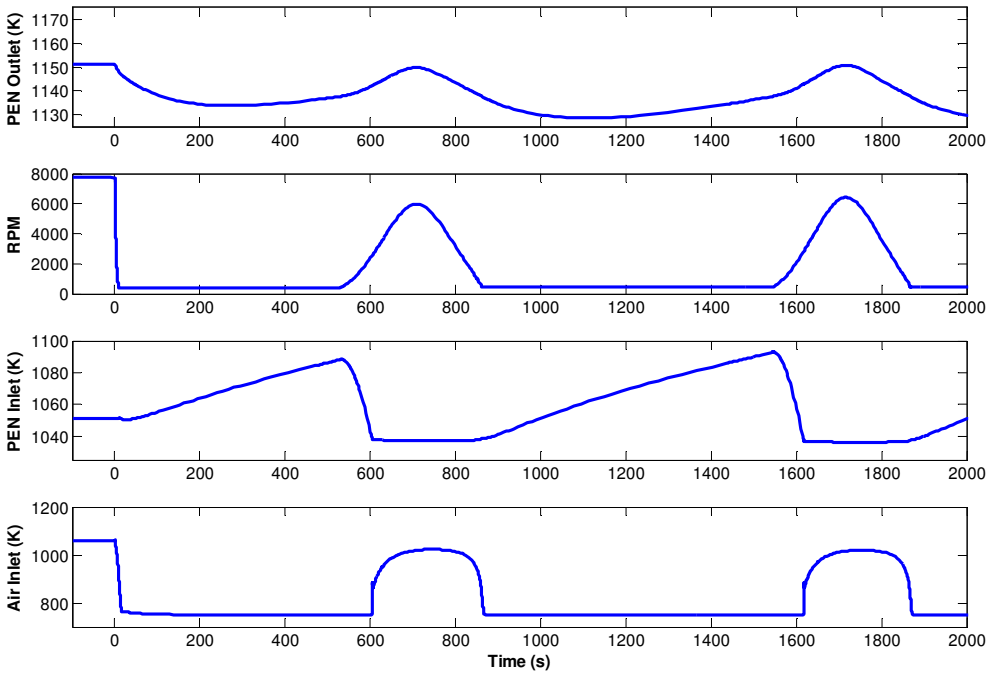

Figure 9 Actuator interaction and saturation resulting in instability following a 5.5 kW to 3 kW load decrease (bypass paired with PEN inlet temperature and blower paired with PEN outlet temperature)

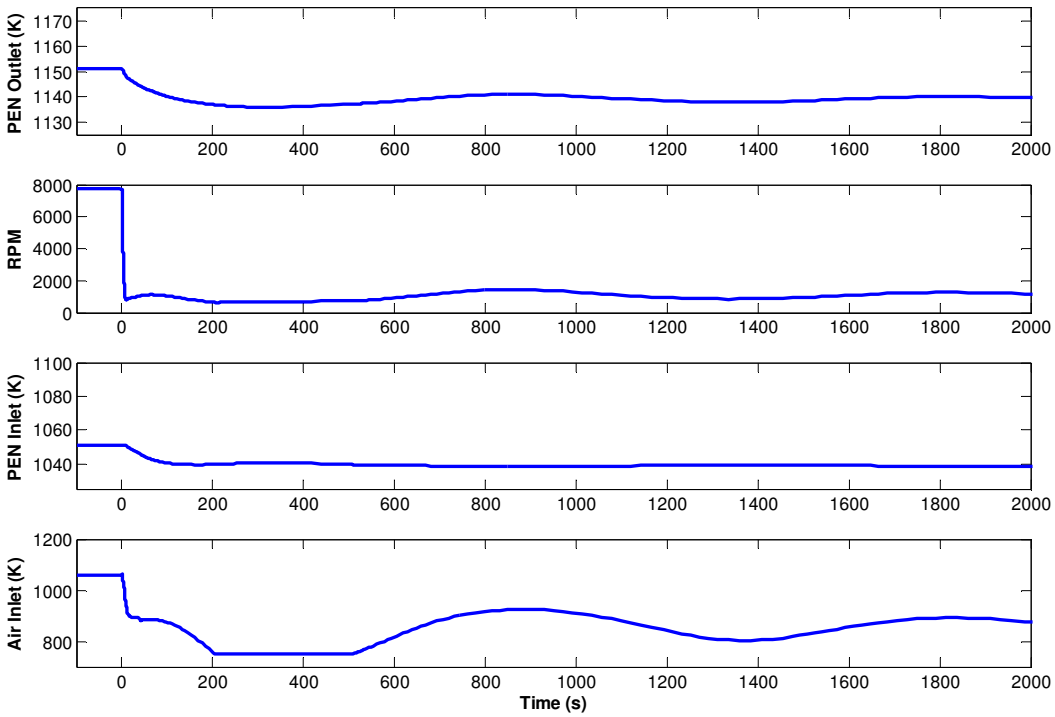

Figure 10 System performance to a load decrease with improved input output pairing (bypass paired with PEN inlet temperature and blower paired with average PEN inlet and outlet temperature).

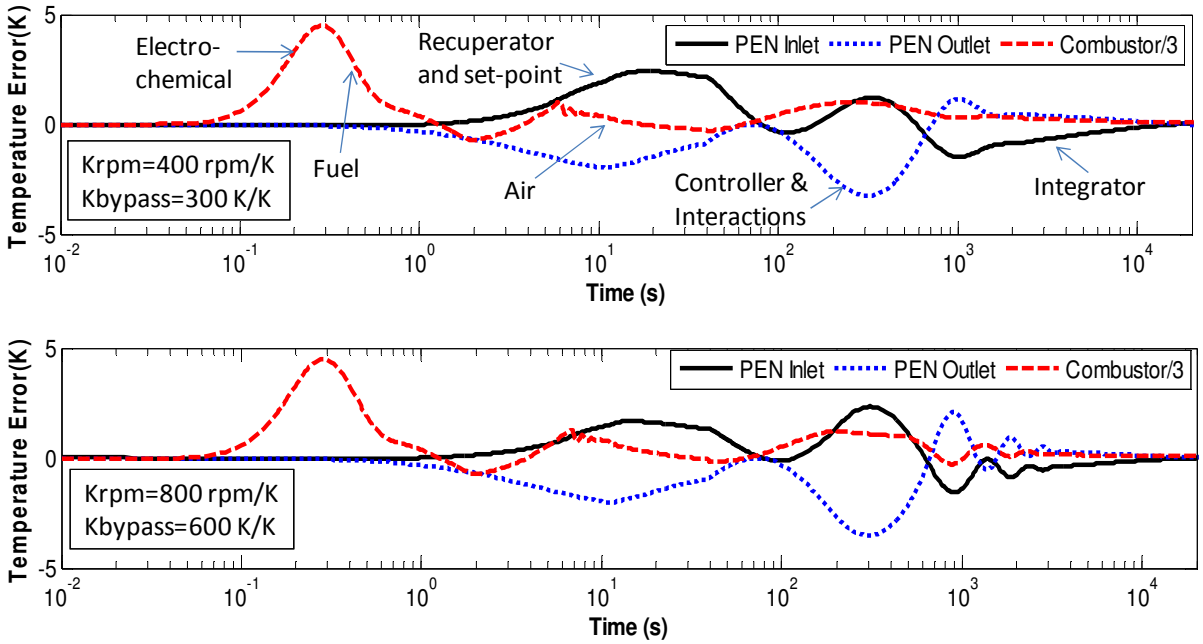

Figure 11 System response to a 3 to 5.5 kW load decrease; sensitivity to feedback gain.

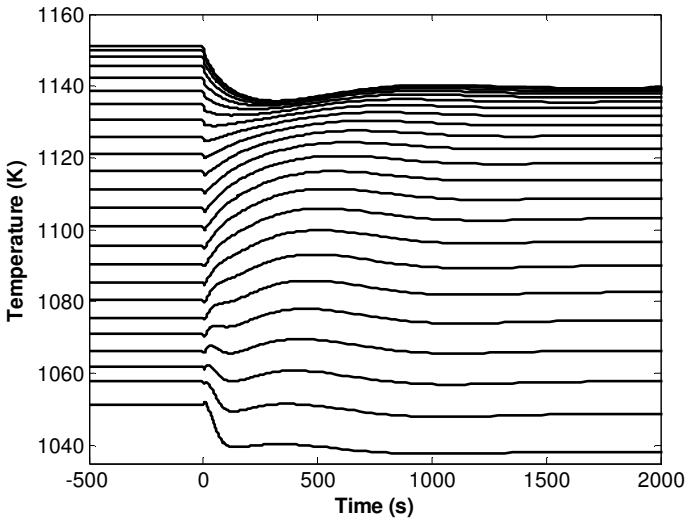

Figure 12 Nodal PEN temperature response to a 5.5 to 3 kW load decrease

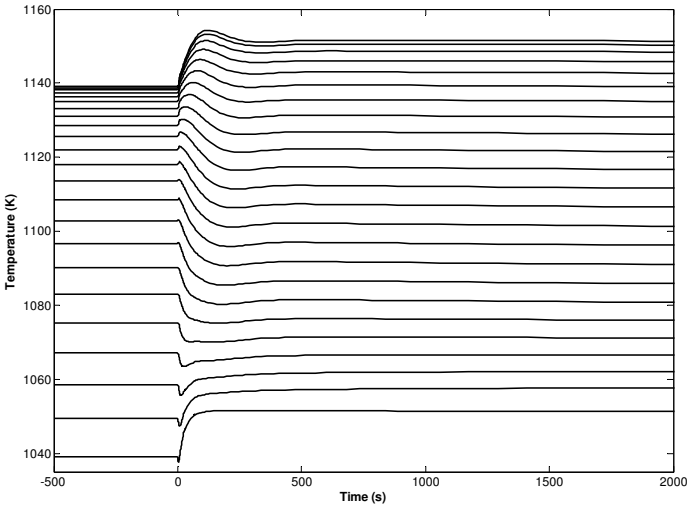

Figure 13 Nodal PEN temperature response to a 3 to 5.5 load increase

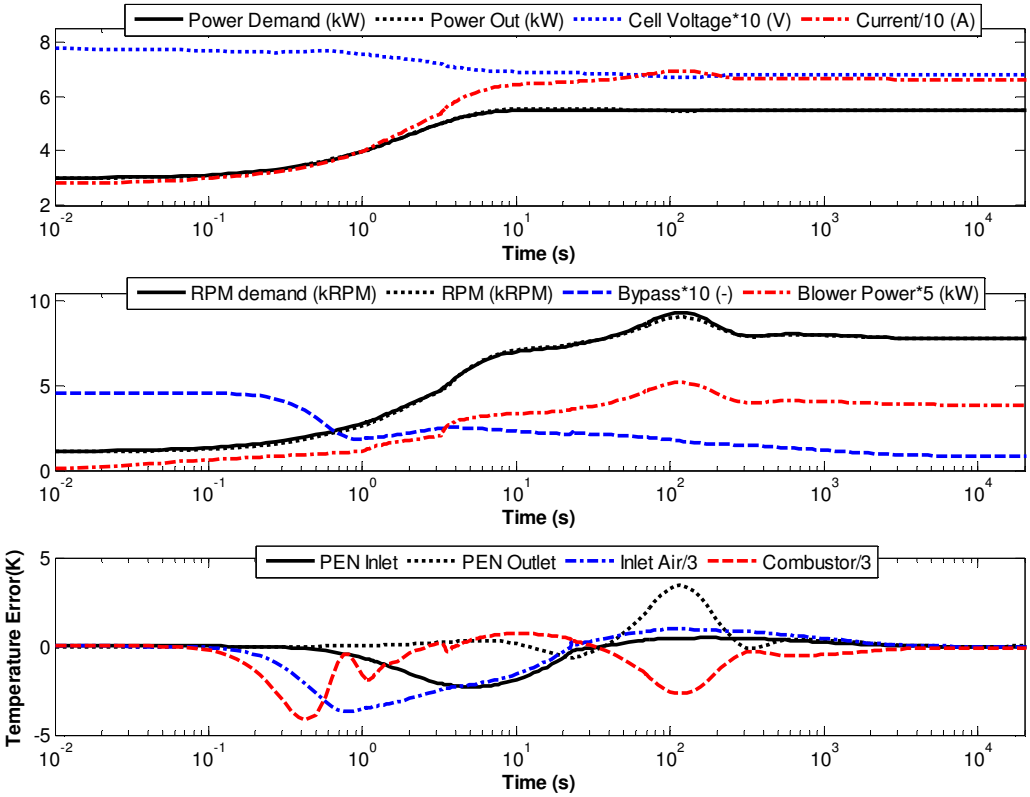

Figure 14 System performance to a 3 to 5.5 kW load increase